Mon. Not. R. Astron. Soc. **363,** 1111–1124 (2005) doi:10.1111/j.1365-2966.2005.09489.x

Tycho-2 stars with infrared excess in the *MSX* Point Source Catalogue

A. J. Clarke,★ R. D. Oudmaijer★ and S. L. Lumsden★
School of Physics and Astronomy, University of Leeds, Leeds LS2 9JT

Accepted 2005 August 2. Received 2005 July 22; in original form 2005 April 20

ABSTRACT

Stars of all evolutionary phases have been found to have excess infrared emission due to the presence of circumstellar material. To identify such stars, we have positionally correlated the infrared *Mid-Course Space Experiment* (*MSX*) Point Source Catalogue and the Tycho-2 optical catalogue. Near–mid-infrared colour criteria have been developed to select infrared excess stars. The search yielded 1938 excess stars; over half (979) have never previously been detected by *IRAS*. The excess stars were found to be young objects such as Herbig Ae/Be and Be stars, and evolved objects such as OH/IR (infrared) and carbon stars. A number of B-type excess stars were also discovered whose infrared colours could not be readily explained by known catalogued objects.

Key words: circumstellar matter – stars: early-type – stars: evolution – stars: pre-main-sequence.

1 INTRODUCTION

The discovery of excess far-infrared (FIR) emission from α Lyrae by the *Infrared Astronomical Satellite* (*IRAS*) by Aumann et al. (1984) demonstrated for the first time that protoplanetary material around other stars could be both detected and studied. Further studies of *IRAS* point sources revealed that many types of star displayed strong emission at *IRAS* wavelengths. This excess is mostly due to thermally reradiating circumstellar dust or, mostly in the case of hot Be stars, due to free–free and bound–free emission from their ionized gaseous discs. Consequently, the *IRAS* Point Source Catalogue (PSC; Beichman et al. 1988) became a much used source for the search and identification of stars surrounded by circumstellar material. The use of an *IRAS* two-colour diagram to systematically identify evolved stars in the *IRAS* PSC, was developed and undertaken by van der Veen & Habing (1988) and Walker & Cohen (1988). They found that the majority of the infrared (IR) excess stars were carbon- or oxygen-rich asymptotic giant branch (AGB) stars undergoing mass loss. Other studies by Plets et al. (1997) and Jura (1999) also discovered giant and first ascent red giant stars with IR excess.

Another manner of finding objects was to use optical catalogues and cross-correlate those with the *IRAS* PSC. Systematic studies, such as those by Pottasch et al. (1988), Stencel & Backman (1991) and Oudmaijer et al. (1992), proved very successful in returning all well-known Vega-type systems and, in addition, uncovering large numbers of both young and evolved stars alike. For example, the presence of IR excess became one of the defining characteristics of pre-main-sequence Herbig Ae/Be stars, and evolved post-AGB stars where the AGB mass-loss phase had ended and the IR excess traces the cool, detached dust shell; see, for example, the reviews by van Winckel (2003) on post-AGB stars, Zuckerman (2001) on dusty discs and Waters & Waelkens (1998) on Herbig Ae/Be stars.

However, the relatively large beam size of *IRAS* (45×270 arcsec^2 at 12 μm and larger at longer wavelengths) meant that regions such as the Galactic plane could not be studied properly because of source confusion. In addition, due to its orbit, the *IRAS* satellite also did not observe 4 per cent of the sky. These so-called '*IRAS* gaps' have never been surveyed in the mid-IR.

The *Mid-Course Space Experiment* (*MSX*) satellite carried out a mid-IR survey of the Galactic plane and other areas of the sky missed by *IRAS* using the SPIRIT III instrument (full details in Price et al. 2001). The sensitivity of SPIRIT III at 8 μm is comparable to *IRAS*, but its beam size is approximately 35 times smaller (at the longest wavelength) and is therefore much less hampered by source confusion. It discovered 430 000 objects in the Galactic plane (defined as $|b| < 6^\circ$), which is four times as many as *IRAS* detected in this region of the sky. Moreover, it surveyed the *IRAS* gaps for the first time in the mid-IR.

The *MSX* survey thus provides an excellent opportunity to systematically search the Galactic plane and the *IRAS* gaps for IR excess stars. The purpose of the present paper is to find optically bright objects within the *MSX* PSCs that were previously unknown as having IR excess. The resulting list can then be used for (optical) follow-up studies. The methodology we adopt is similar to that of Oudmaijer et al. (1992). They cross-correlated the optical Smithsonian Astrophysical Observatory (SAO) catalogue with the *IRAS* PSC, to identify objects with IR excess. The FIR colours immediately reveal non-photospheric emission if the temperatures are less than about 200 K while those objects with higher colour temperatures are identified by assessing the IR fluxes compared to that

★E-mail: ajc@ast.leeds.ac.uk (AJC); roud@ast.leeds.ac.uk (RDO); sll@ast.leeds.ac.uk (SLL)

predicted from the photospheric optical emission. After a further selection on spectral type (BAFG – typical for most evolved and young stars) this search revealed a master sample of 462 objects. As *MSX* did not observe beyond 20 μm, it is not readily possible to find excess objects based on *MSX* data alone, and we will rely on computing the IR excesses using additional information to identify the stars of interest. Rather than use the SAO catalogue, we will use the much larger optical Tycho-2 catalogue (Hog et al. 2000) and its accompanying spectral type catalogue (Wright et al. 2003), which contains more than 350 000 spectral types as a starting point. To further characterize the IR emission of any objects found, we will also use data from the Two-Micron All-Sky Survey (2MASS) catalogue of point sources (hereafter 2MASS PSC; Cutri et al. 2003).

This paper is organized as follows. In Section 2 we describe the initial input catalogues and the cross-correlation of the Galactic plane sample in detail. In Section 3 we discuss the properties of the resulting sample and develop a new method of identifying IR excess stars. We end with a discussion of the resulting final sample of excess stars and outline the way it is presented. We also discuss in Appendix A the application of the excess identification procedure to the *MSX IRAS* gap survey and other regions surveyed by the *MSX* mission.

2 INPUT DATA AND CROSS-CORRELATION

In order to define an IR excess for the sample stars, we use the *MSX* mid-IR catalogue, the optical Tycho-2 catalogue and the near-IR 2MASS PSC. As will be shown later, once the 'optical' stars have been identified, the use of their near-IR magnitudes has marked advantages over using the optical data alone. Below, we describe the input catalogues and Galactic plane cross-correlation in detail. The other *MSX* catalogue cross-correlations will be discussed in Appendix A.

2.1 Data sources

The *MSX* SPIRIT III instrument observed in six photometric bands between 4 and 21.34 μm, and was most sensitive at 8.3 μm where its sensitivity was comparable to the *IRAS* 12-μm band. The *MSX* mission surveyed the Galactic plane, *IRAS* gaps, Magellanic Clouds as well as some other regions of high stellar density. A major data product of the *MSX* mission was the *MSX* PSC v2.3 (hereafter *MSX* PSC; Egan, Price & Kraemer 2003), which has a positional accuracy, $\sigma = 2$ arcsec, and a limiting flux at 8 μm of 0.1 Jy.

As we wish to identify a large sample of new IR excess stars, we require a sufficiently large and accurate optical star catalogue. For this reason we used the Tycho-2 star catalogue compiled from data collected by the Tycho star mapper on-board the *Hipparcos* astrometric satellite. The positional accuracy of Tycho-2 is excellent and more than required for our cross-correlation purposes. The completeness limit (99 per cent) of the catalogue is given as 11 in the V_T band, and its limiting magnitude is about 14 in the V_T band and 15 in the B_T band. Tycho-2 observed objects many times, resulting in a photometric precision of typically 0.05 mag. Obviously, this precision becomes worse at the fainter end; for magnitudes around 10–11 the photometric error is 0.1 mag rising to 0.3 mag close to the detection limits.

The Tycho-2 catalogue does not contain any stars brighter than $B_T < 2.1$ or $V_T < 1.9$ due to the nature of the data reduction technique. We used the brighter stars from the first supplement to the Tycho-2 star catalogue.

Near-IR photometry is taken from the 2MASS PSC, which contains nearly half a billion sources. The survey is complete to magnitude $K \sim 15$. The data have relatively bright saturation limits ($K \sim 3.5$), although for $K < 8$ the 2MASS catalogue lists photometry estimated from radial profile fitting to the wings of the saturated sources. The photometric accuracy, especially at the fainter end, is better than that of Tycho-2, and for bright saturated sources comparison with previous observations suggests the error is typically <10 per cent.

Finally, to learn more about the sample, spectral type information is very important. Wright et al. (2003) compiled all known spectral classifications for Tycho-2 stars, and their catalogue contains spectral types for 351 863 stars of which 61 472 are in the Galactic plane (defined here as $|b| < 6^\circ$). As might be expected the objects with spectral types are somewhat brighter on average than the full sample.

2.2 Positional correlation

We have positionally correlated the Tycho-2 star catalogue and the *MSX* v2.3 PSC. For a positional association between a Tycho-2 star and an *MSX* source, the separation of the two objects is required to be less than 6 arcsec, corresponding to a typical 3σ accuracy of the *MSX* position. In the case of two stars within 6 arcsec of an *MSX* source we have taken the closest.

The deviations of the *MSX* positions compared to the Tycho-2 positions in the right ascension and declination directions are centred at zero with $\sigma = 2$ arcsec, indicating that, in a statistical sense, the Tycho-2 and *MSX* associations are real. The shape of the distribution compared well with the similar in-scan and cross-scan separation distributions shown by Egan et al. (2003). To test the 6-arcsec cut-off, the correlation was extended out to a radius of 15 arcsec. We found that the majority (90 per cent) of the associations had separations smaller than 6 arcsec and the distribution showed that at larger radii the number of associations reached some random background level. We therefore concluded that 6 arcsec was the optimum value for the cut-off for positional association.

The *MSX*–Tycho-2 sources have also been further correlated with the 2MASS PSC, using a 6-arcsec search radius around the *MSX* position. In the case of multiple 2MASS sources within the 6-arcsec search radius, we have taken the closest match and flagged the *MSX* source.

To ensure that all *MSX*–2MASS counterparts are also Tycho-2–*MSX*–2MASS associations, we require the 2MASS source to be additionally within 0.50 arcsec of the Tycho-2 catalogue position. Failing to do the latter returns many sources that are either unrelated to the *MSX* or the Tycho-2 source and would severely contaminate the final sample.

We made use of the Infrared Science Archive (IRSA)[1] to perform the 2MASS cross-correlations.

2.3 Photometric constraints

At this stage we made certain requirements of the photometry provided by the different catalogues for further inclusion in the sample so the presence of the IR excess is credible/significant. For the Tycho-2 star catalogue we required that a star be detected at both the

[1] See http://irsa.ipac.caltech.edu.

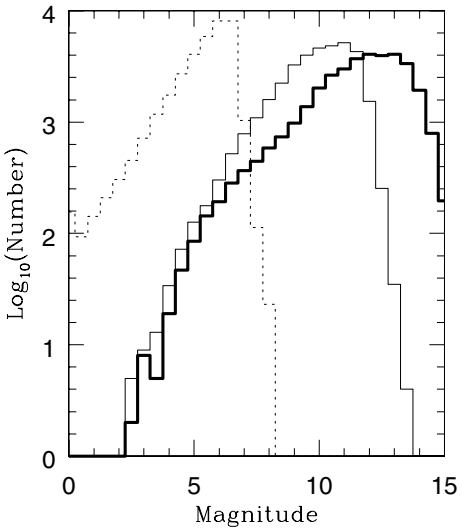

Figure 1. The magnitude distribution of the Galactic plane sample in the optical and mid-IR. The optical B_T and V_T bands are represented by the thick and faint solid lines, respectively. The *MSX* 8-μm distribution is indicated by the dashed line.

B_T and V_T bands (corresponding to magnitudes of less than 15 and 14 in B_T and V_T, respectively, according to the Tycho-2 explanatory supplement; Hog et al. 2000). For the *MSX* data we required a detection in at least one band with flux quality greater than 1 (signal-to-noise ratio greater than 5). The only constraint we made on the 2MASS photometry is that it must be better than an upper limit (i.e. not having a U or X flag) at all bands.

2.4 Galactic Plane

The *MSX* PSC (v2.3) Galactic plane $|b| \leqslant 6^\circ$ survey (including the plane regions of the *IRAS* gaps) contains 431 711 sources. After cross-correlation with the Tycho-2 optical star catalogue, we are left with 35 044 (≈8 per cent) associations which meet our photometric constraints. The bulk (≈75 per cent) of these Galactic plane sources were only detected at the most sensitive *MSX* band A (8.28 μm). The further correlation of the *MSX*–Tycho-2 sources with the 2MASS PSC search found 33 495 (95 per cent) counterparts. A small fraction of these (3 per cent) had multiple 2MASS sources within the *MSX* search area; in these cases we cannot rule out the possibility that the *MSX* source is actually a nearby optically invisible 2MASS source rather than the Tycho-2 star. A clear example of this is the B-type star HD 93942 (the object with K–[8] ≈ 8 in Fig. 4, later) which is in close proximity to a very red (optically invisible) carbon star. In the near-IR there are two 2MASS sources within 6 arcsec of the *MSX* source position. Although the *MSX* flux is most likely from the carbon star, it is difficult to determine which of the 2MASS sources is the correct association. As we cannot objectively remove these sources, we flag them.

Using the magnitude distribution of the sample (see Fig. 1) we estimate the sample is complete to magnitude 8 in V_T, 11 in B_T and 5 in *MSX* Band A (or [8] hereafter).[2] This makes it the most complete IR sample of optical stars in the Galactic plane to date. Of the 35 044 Tycho-2–*MSX* sources described above, about a third, 12 783, are listed in the Tycho-2 spectral type catalogue. A smaller fraction of these, 7443, have two-dimensional spectral types.

2.5 Comparison with *IRAS*

To ascertain how many of our sources have previously been detected with *IRAS* and hence estimate how many objects in our final sample are new identifications, a positional correlation of the *MSX*–Tycho-2 sources with the *IRAS* PSC (Beichman et al. 1988) has also been undertaken. We used the VizieR[3] catalogue access tool to search the *IRAS* PSC around the *MSX* positions of our *MSX*–Tycho-2 associated stars. For the correlation we used a circular search radius of 45 arcsec, typically corresponding to three times the major axis of the elliptically shaped *IRAS* 1σ positional uncertainties (Beichman et al. 1988).

Of the 35 044 *MSX*–Tycho-2 sources, 9473 were found to be within 45 arcsec of an *IRAS* source. We therefore conclude that the majority of any IR excess stars in this paper are new identifications and previously unstudied.

3 RESULTS FOR THE GALACTIC PLANE

In the following we first discuss the properties of the sample using colour–colour diagrams, and then continue with the identification of excess stars. In order to do this, we first derive a relationship between the near-IR colours and the *MSX* 8-μm magnitude for normal stars. We concentrate on the largest *MSX* catalogue, that of the Galactic plane, and briefly discuss the selection from the other samples later.

3.1 General properties

Fig. 2 shows a (B_T–V_T, V_T–[8]) colour–colour diagram[4] which is the *MSX* analogue to the well-studied diagnostic *IRAS* (B–V, V–[12]) diagram (e.g. Waters, Coté & Aumann 1987a, hereafter WCA).

The left-hand panel, containing all objects, shows a main band with increasing spread around it towards redder colours; the objects with known spectral types are plotted in the right-hand panel. Not surprisingly, this subsample is on average brighter, and a large number of objects has dropped out, allowing us to recognize a well-defined band in the plot. The larger spread evident in the full sample is thus mostly due to larger photometric errors.

This diagram is a good diagnostic to identify IR excess stars, as originally described by WCA. Normal stars follow a well-defined sequence, while objects with excess 8-μm emission are readily identified by their deviating V_T–[8] colours. This is also observed here; the 'main band' of stars follows a more or less well-defined relation and is accompanied by objects located above this relation. These are the IR excess stars; the majority of stars in the Tycho-2-*MSX* sample are not IR excess stars but normal stars.

[2] The *MSX* fluxes are converted to magnitudes using zero-point fluxes from Egan et al. (2003), which is 58.49 Jy at 8 μm.

[3] See http://vizier.u-strasbg.fr.

[4] On each diagram the magnitude and direction of a typical interstellar extinction vector are indicated and calculated using the following assumptions. For the mid-IR wavelengths ($\lambda > 5$ μm) we have used the *MSX* filter averaged astronomical silicate data (Draine & Lee 1984) as derived by Lumsden et al. (2002). For the near-IR wavelengths ($\lambda < 5$ μm) we adopt an extinction law that varies as $\lambda^{-1.75}$. For the optical bands we have used the standard optical $A_V = 3.1[E(B-V)]$ extinction relation.

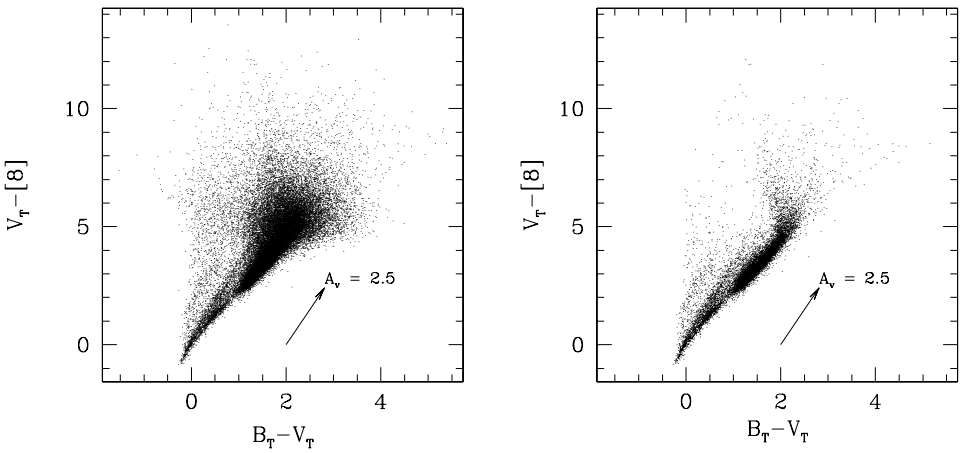

Figure 2. Optical–mid-IR colour diagram of the sources. The horizontal axis denotes the Tycho B_T–V_T colours, while [8] represent the *MSX* 8-μm magnitude (see text). The left-hand panel shows all 35 030 *MSX* sources with a Tycho counterpart. The right-hand panel shows the 12 778 objects with known spectral types. Note that this (brighter) sample shows a smaller spread around the main band. For comparison, a reddening vector is also shown.

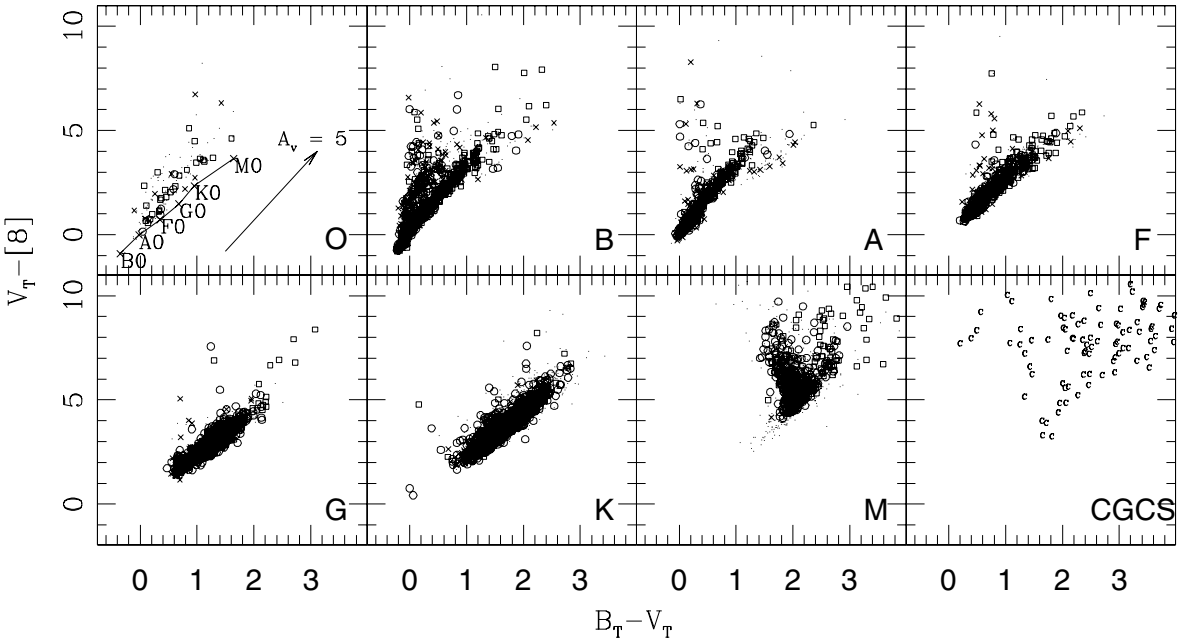

Figure 3. Optical and mid-IR colour diagram showing the different regions occupied by different spectral type stars. The spectral type is shown in the lower right-hand corner of the respective panel. The samples consist of 125 O-type stars, 1003 B stars, 718 A stars, 943 F stars, 2288 G stars, 6495 K stars and 1099 M stars. Stars with CGCS identifications are also shown. The luminosity class of the stars is represented by the following symbols: squares, I, II; circles, III, IV; times symbols, *V*; with unclassified stars indicated by a dot. The intrinsic colours of dwarf stars (see text for details) together with the extinction vector to indicate the degree of reddening of the sample are also shown in the upper left-hand panel.

3.2 Excess as a function of spectral type

To further investigate the properties of the sample, we plot the colour–colour diagrams for each spectral type in Fig. 3. The sample is broken down into the spectral types O–M while a set of carbon stars, taken from the Catalogue of Galactic Carbon Stars (CGCS; Alksnis et al. 2001), is also shown. Where known, dwarfs (luminosity class V), giants (IV–III) and supergiants (I–II) are indicated by different plot symbols. As a guide for the intrinsic colours of main-sequence stars in Fig. 3 we show the median V_T–[8] colours of B0 to M0 dwarf stars taken from Cohen, Hammersley & Egan (2000), plotted against the intrinsic *B*–*V* colours of these stars given by Schmidt-Kaler (1982), which are corrected for Tycho photometry using the transformations given in the *Hipparcos* and Tycho catalogues (1997).

The earlier-type stars are dominated by main-sequence stars, while giants constitute the majority for the later-type objects as the dwarfs are too faint to be detected in both optical and IR catalogues. The transition between dwarfs and giants is visible as the relative paucity of sources at B_T–$V_T \approx 0.75$.

A separate bifurcation is also visible at B_T–$V_T \approx 1$ in Fig. 2. The upper sequence consists of reddened supergiants while the lower sequence consists of giants (and some dwarfs). This separation of luminosity classes (beginning at early G type) was first noted by

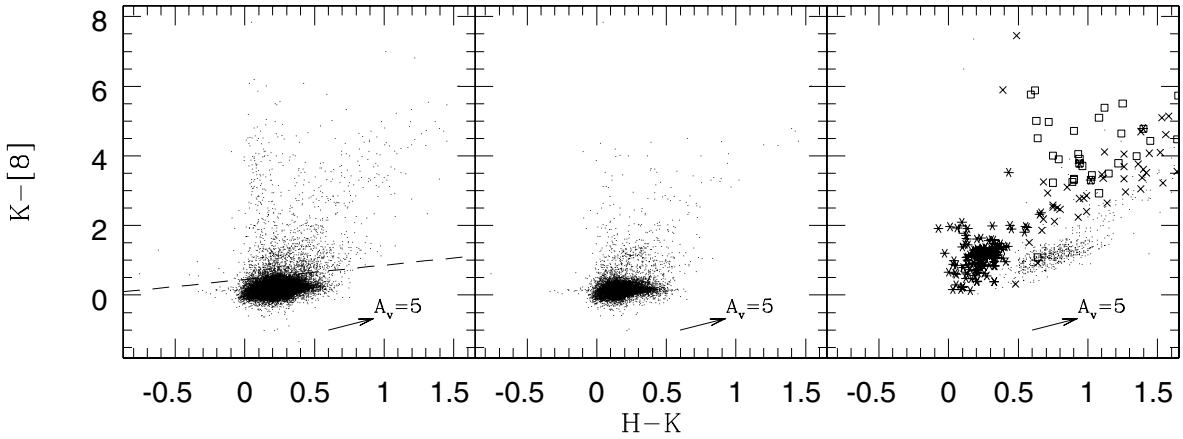

Figure 4. Near–mid-IR (left) colour diagram of *MSX*–Tycho-2–2MASS sources (33 485), with (centre) spectral type (12 452) and (right) the colours of known sources (not necessarily in our sample). The excess cut-off line is shown in the left panel (see text for details). The symbols in the right-hand panel indicate the type of objects: asterisks, a Be-type star from our sample; times symbols, an OH/IR star; squares, a Herbig Ae/Be star. A dot indicates an optical carbon star.

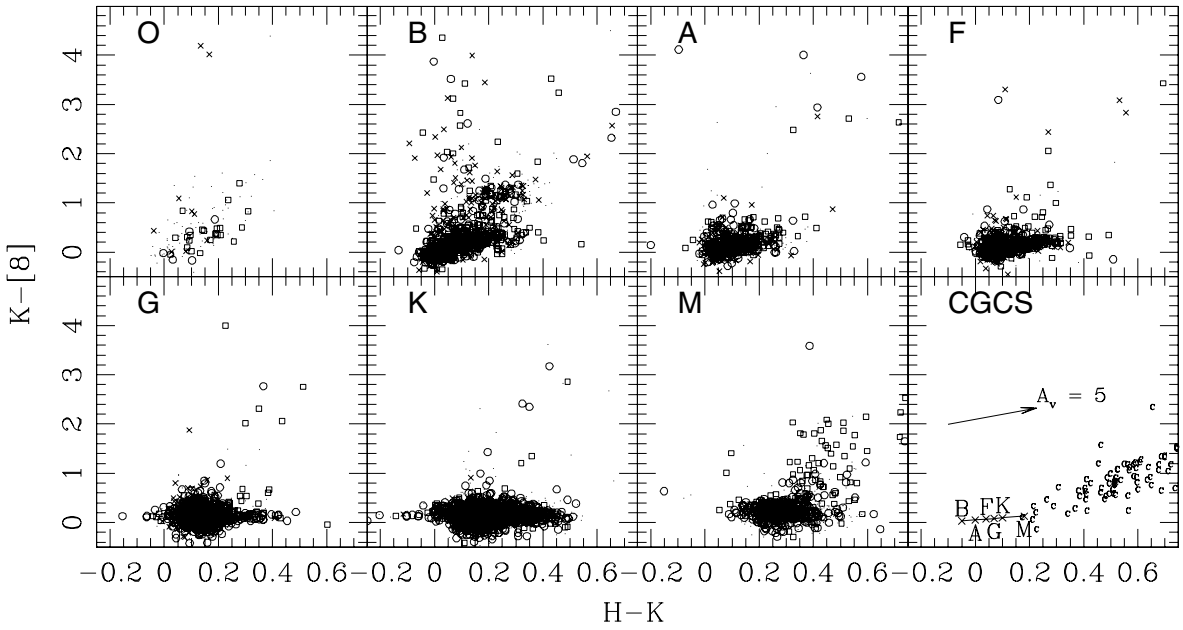

Figure 5. Near–mid-IR colour diagram showing the different regions occupied by different spectral type stars. The spectral type is shown in the upper left-hand corner. The samples consist of 120 O-type stars, 937 B stars, 672 A stars, 885 F stars, 2219 G stars, 6406 K stars and 1086 M stars. Stars with CGCS identifications are also shown. The luminosity classification of the stars is represented by the following symbols: squares, I, II; circles, III, IV; times symbols, V. Unclassified stars are indicated by a dot. The intrinsic colours of dwarf main-sequence stars (see text for details) together with the extinction vector to indicate degree of reddening of the sample are also shown in the lower-right panel.

Cohen (1987) in the *IRAS V*–[12] diagram. A property apparent for all spectral types is that the non-excess stars span a much wider $B_{\rm T}$–$V_{\rm T}$ range than the intrinsic colours for the respective types signal. This is due to the presence of a large interstellar reddening at low galactic latitudes, and is illustrated by the reddening vector indicated in the diagram. The main bands defined by non-excess stars per spectral type are parallel to the extinction, and correspond to values up to $A_V \sim 5$. Often the reddest objects are supergiants, which is also consistent with reddening; the objects with the largest extinction are presumably at the largest distances and therefore have to be intrinsically brighter.

For the B-type stars, and also, but less obvious, for the O stars due to the lower number of stars involved, the colour diagram is dominated by two bands which are both populated by main-sequence stars. The lower band contains normal, non-excess objects, and the upper band is populated by a large number of excess stars, many of which are Be stars. The excess emission is explained by free–free emission from the ionized gas in the circumstellar disc (Water, Coté & Lamers 1987b). The relative number of A-type excess stars is much smaller, and seems to consist of dwarfs and supergiants in roughly equal numbers. There would seem to be a special class of A-type stars around $B_{\rm T}$–$V_{\rm T} = 1.5$, where these seem to branch off at a different slope than the other A-type stars. It appears however that these objects have colours similar to K-type stars and the most likely explanation for this is that their spectral types are misclassified or that they are binaries with a K-type counterpart.

The F-, G- and K-type stars have fewer excess objects. The M star sample shows a distinct upturn. As already noted by WCA, for these cool objects, the optical colours probe the Wien part of the spectral energy distribution and show hardly any dependency on temperature any more. The 8-μm band is sensitive to spectral features, such as molecular bands, and therefore shows a strong gradient. This particular colour diagram is thus not a useful diagnostic to identify M stars with IR excess.

Perhaps unsurprisingly, the carbon stars follow a similar band as the M stars. However, the relatively large photometric uncertainties of these faint stars mean they sometimes appear at much bluer colours than would normally be expected.

It is important to highlight a significant difference with previous studies here. WCA, in particular, but also Oudmaijer et al. (1992), used optical catalogues with brighter cut-offs – the Bright Star Catalogue (Hoffleit & Warren 1991) and the Smithsonian Astrophysical Observatory star catalogue (SAO Staff 1966) with limits $V = 7$ and 9–10, respectively – than used here. The deeper Tycho-2 sample inevitably contains a large fraction of (heavily) reddened stars, which is aggravated by the fact that we observe in the direction of the Galactic plane. It can be seen in the upper-left panel of Fig. 3 that the extinction vector is non-parallel to the 'normal star' relation. This gives heavily reddened normal stars V_T–[8] colours similar to excess stars. Moreover, the fainter, numerous, Tycho-2 stars have comparatively large photometric errors (as indicated by the large spread in Fig. 2), making it harder to recognize excess emission from the optical-IR colour–colour diagram. It is therefore not trivial to properly identify stars with excess from the Tycho-2–*MSX* data alone. Therefore, to make headway, we need to go to wavelengths where the extinction will be less – the near-IR.

3.3 Near-infrared

To reduce the impact of extinction on the IR excess star selection, we show the near- and mid-IR colour equivalent to Fig. 2 in Fig. 4. The K–[8] range spanned by the normal stars is much smaller than the V_T–[8] range because we now probe the Rayleigh–Jeans tail of the spectral energy distribution for all stars. The H–K colour range is small for the same reason, while the reddening is less severe – typically $E(H-K) = 0.22\ E(B-V)$. Most of the objects beyond $H-K > 0.5$ suffer from reddening, and also objects with excess emission at K give rise to red H–K colours.

To understand and describe the features of the colour diagram, we have also plotted the colours of known objects (Fig. 4) which have been observed by *MSX* (but are not necessarily part of the Tycho-2 sample). The objects plotted are from the following catalogues: optical selected carbon stars from Alksnis et al. (2001), OH/IR stars (AGB stars with large mass-loss rates) from Chengalur et al. (1993), Herbig Ae/Be stars from Thé, de Winter & Perez (1994) and the Be-type stars extracted from our own Tycho-2 sample (which were found to agree with the mid–near-IR colours of all known Be stars as compiled by Zhang, Chen & Yang 2005).

The distribution of B stars with excess in Fig. 5 shows a clearly defined band of excess stars with K–[8] < 2 and a more diffuse distribution of stars with greater excess emission, which is further complemented by a large number of excess stars without spectral classification (see Fig. 4).

It is immediately apparent from Fig. 4 that only the B stars with K–[8] < 2 can be explained by the properties of the known Be stars. The remaining objects with greater excess emission are therefore very interesting; we discuss in Section 5 the possible nature of these objects.

The two branches beginning at $H-K = 0.50$, with gradients roughly equal to the reddening vector, are clearly associated with the carbon and OH/IR stars. The OH/IR stars also have a slightly greater (1 mag) K–[8] colour, presumably due to their higher mass-loss rates over these optically selected carbon stars. The Herbig Ae/Be stars all show excess emission and are heavily reddened, due to their surrounding circumstellar material.

Spot checks on stars with $H-K < 0$ revealed the majority have saturated K-band magnitudes, and therefore their colours are just affected by the resulting error bar. The objects with K–[8] < −0.50 are, in general, variable stars and binaries.

Although we plot the same number of objects in Figs 2 and 4, the excess stars are more easily distinguishable than in the optical diagram. In addition to the reduced extinction, this is also the case because of the smaller photometric error bars involved, validating the use of near-IR colours.

The distribution over spectral type is shown in Fig. 5. All features described for the optical (Fig. 3) are present, but much more prominent. It is clear that the near–mid-IR two-colour diagram is a much better tool for the selection of IR excess stars, due to the removal of the strong extinction effect and the better photometric accuracy of 2MASS for the optically fainter objects. We therefore proceed with this colour diagram to identify IR excess stars.

3.4 $H-K$, K–[8] relation for normal stars

To identify stars with excess 8-μm emission, we first need to know the photospheric contribution for all stars at this wavelength. To derive this, we adopt the iterative procedure used by WCA for *IRAS* sources. This involves dividing the sample into H–K colour bins (0.01 mag width in our case) and calculating the mean $(K-[8])_{av}$ and standard deviation σ of the bin. By eliminating the outliers (defined as deviating by more than 2σ from the mean), this process was repeated until the $(K-[8])_{av}$ no longer changed significantly with further iterations.

The procedure was only run over the intrinsic main-sequence near-IR colours given by Koornneef (1983) ($H-K = -0.05\ldots 0.45$). This step essentially removes the heavily extincted sources, whose IR colours are heavily distorted by reddening. The final $(K-[8])_{av}$ values could then be well fitted by the following straight line:

$$(K-[8])_{photo} = 0.41(H-K)_* + 0.05. \quad (1)$$

This photospheric relation was extrapolated to cover the entire range of (H–K) colours spanned by the sample stars. Using this relation and the intrinsic main-sequence near-IR colours quoted by Koornneef (1983), we derive a relationship between the spectral type of a star and its K–[8] colour (as shown in the lower-right panel of Fig. 5).

4 TYCHO-2 STARS WITH INFRARED EXCESS

In this section we select the excess stars. We first discuss the more numerous 8-μm excess stars, and then discuss excess at the other *MSX* wavelengths.

4.1 Stars with warm dust: excess 8-μm emission objects

To calculate the IR excess emission of the stars in our sample we follow Oudmaijer et al. (1992), who used the relationship between

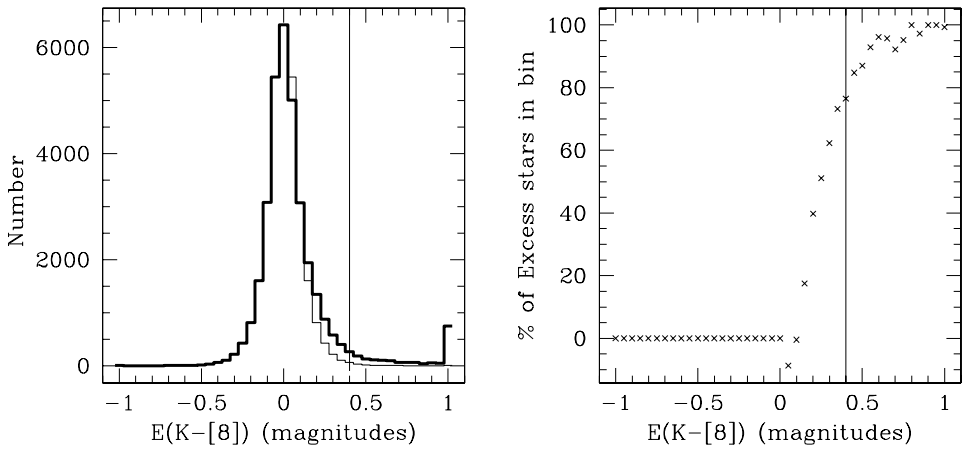

Figure 6. Excess K–[8] $E(K$–[8]) distribution of sample; the negative excess distribution is mirrored through $E(K$–[8]) = 0 to illustrate the asymmetry of the distribution. The right-hand panel shows the percentage of excess stars as a function of $E(K$–[8]) emission. The excess definition threshold is also shown at 0.40 mag.

the photospheric colours in the optical and *IRAS* 12 μm for normal stars. With the expression of the intrinsic K–[8] colour for normal stars already in hand, it is trivial to compute the excess 8-μm emission. Expressed in magnitudes this is done by $E(K\text{–}[8]) = (K\text{–}[8]) - (K\text{–}[8])_{\rm photo}$.

The main issue is to decide on where to choose the cut-off for inclusion into the final sample of IR excess stars. In Fig. 6 we show a histogram of the excesses in magnitudes. The distribution of $E(K$–[8]) is asymmetric about zero. The negative excesses show a Gaussian shape. The positive side also displays an underlying Gaussian distribution, with a large non-Gaussian tail that contains the excess stars. The Gaussian shape on the negative side is explained simply by the width of the observed sample in the H–K K–[8] colour diagram. The width (FWHM = 0.20) in this case is dominated by the photometric error in the *MSX* 8-μm flux (5–20 per cent) rather than the intrinsic scatter of normal non-excess stars.

We can now derive the fraction of objects with excess 8-μm emission. By using the negative excess distribution (assumed to be symmetric around zero) as an estimate of the non-excess distribution, we can calculate the percentage of excess stars as a function of $E(K$–[8]). This is shown in Fig. 6. The percentage of excess stars is zero for the negative side (by definition) and rises relatively quickly to 100 per cent at $E(K$–[8]) = 0.80. We choose to have at least an 80 per cent probability of IR excess in our sample. This corresponds to a $E(K$–[8]) cut-off of 0.40 mag.

Using these criteria we identify 1830 8-μm excess stars in our sample, around half of which (965) are not within 45 arcsec of an *IRAS* point source and are therefore new identifications. We also identify one excess star which was too bright to be included in the Tycho-2 catalogue (and hence was picked up in the Tycho-2 supplement), the well-known Be star γ Cas.

4.2 Stars with hot dust: K-band excess emission objects

It should be noted that the above procedure selects objects that have excess 8-μm emission relative to the K band. An object surrounded by only hot dust will not be selected as its 8-μm emission has a similar K–[8] colour as a cool C- or M-type star. Indeed, the intrinsic

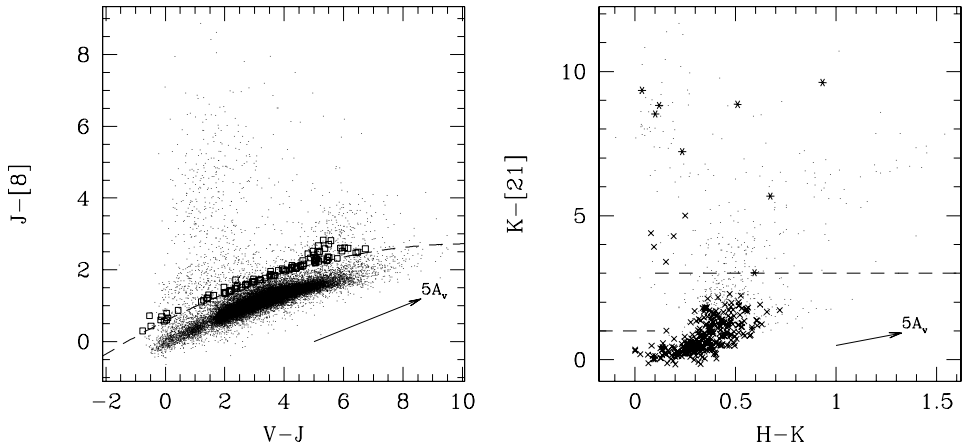

Figure 7. Optical–mid-IR and near–mid-IR colour diagrams showing the J–[8] and K–[21] colours for hot and cold excess emission, respectively. In the left panel, a square indicates a star with excess J–[8] emission but normal K–[8] colours; the rest of the sample is indicated by a dot. The right panel shows the K–[21] colours for cool excess identification. Stars detected at 21 μm but not at 8 μm are indicated by an asterisk; stars detected at both 8 and 21 μm are indicated by a dot if they show excess at 8 μm, or a times symbol if they do not.

K–[8] colour for a 1000–2000 K blackbody is about ∼0.5, and it may well be that such objects will not be selected as their observed K–[8] colour seems to all intents and purposes 'normal'. We therefore need to identify K-band excess stars separately.

We investigated several ways to identify such objects and found the best method is to use V_T–J, J–[8] colours as shown in Fig. 7. This avoids the problem of having the large error bars we encountered in the optical B_T–V_T colours and includes objects with excess even at the H band. It is extremely rare for hot dust to be responsible for J-band excess. Indeed, checks on a random sample of J excess emission objects revealed them to be uncatalogued binary objects, where the J emission is due to a bright cool secondary. We identify the K-band excess stars using a similar iterative procedure as for the K–[8] colours and we derive the following relation for the photospheric contribution:

$$(J\text{–}[8])_{\rm photo} = -0.025 + 0.420(V_T\text{–}J) - 0.021(V_T\text{–}J)^2. \quad (2)$$

The excess J–[8] colour distribution showed that the probability of excess reached 80 per cent at a $E(J\text{–}[8]) = 0.60$ mag and this is where we placed the excess cut-off. This method of excess identification returned only 68 per cent of the K–[8] excess sources and a further 95 stars which do not have excess compared to K at 8 or 21 μm. Interestingly, only nine were not observed by *IRAS*, possibly because the hot excess stars are relatively IR bright.

4.3 Stars with cool dust: 21-μm excess emission objects

Stars such as post-AGB stars surrounded by a cool detached dust shell may not show any distinguishing excess emission at 8 μm. We therefore wish to use the longer wavelength *MSX* bands to identify such sources in our sample. The previous searches for cold excess objects (e.g. Oudmaijer et al. 1992) made use of the *IRAS* FIR colour–colour diagram to identify excess if temperatures are less than 200 K (indicating that IR emission was not photospheric). A similar approach with *MSX* is hampered by the reduced sensitivity of *MSX* at longer wavelengths. Indeed, very few sources (2 per cent) in the sample are detected (i.e. flux quality greater than 1) in every band. As a compromise we will use the K–[21] colour (see Fig. 7) to identify cool excess objects. This has the further advantage that stars detected exclusively at 21 μm are not removed from the sample as they would be if we relied on a multi-*MSX* colour diagram.

Fig. 7 shows the K–[21] colours, of all sources with a flux quality greater than 1 at 21 μm, plotted against H–K. Objects that are found to display 8 μm excess emission are indicated by a dot, while those not detected at 8 μm or not found to have excess are indicated by larger plot symbols. It is immediately apparent that the majority of the cool excess objects also have excess 8 μm emission.

Of the stars without 8-μm excess only a few have K–[21] colours significantly different from the rest of the sample (the majority of which are M giants). All sources that are detected at 21 μm but are not detected in the more sensitive 8-μm band show cool excess emission. To determine the excess cut-off we have used the median V–[25] values published by Cohen (1987) and converted to K–[25] using the appropriate V–K colours from Koornneef (1983). As the [21] and [25] bands both probe the molecular absorption bands of the cool M-type giant stars, we may assume that the K–[25] and K–[21] colours are roughly comparable. We therefore define the excess cut-off to be the 3σ deviation from the intrinsic K–[25] colours of giants. Hence we select stars with cool IR excess if they have $H\text{–}K < 0.1$ and $K\text{–}[21] > 1$ or $K\text{–}[21] > 3$ at $H\text{–}K > 0.1$, as shown in Fig. 7. Using these criteria we identify 13 cool IR excess stars which do not have excess 8-μm emission, five of which do not have *IRAS* counterparts.

5 DISCUSSION

In this paper we have searched for stars with IR excess in the combined Tycho-2, 2MASS and *MSX* catalogues. This resulted in a grand total of 1938 excess stars, of which 979 were not detected by *IRAS* and are thus newly discovered objects.

5.1 Distribution over spectral type

In Fig. 8 we show the number of Tycho-2–*MSX* stars as a function of temperature class. Alongside we also show the percentage of these stars which were found to have excess emission.

We find that the percentage of excess appears to decrease with effective temperature and that the hotter stars (O, B and A) and very cool (M) have a much higher percentage of excess stars than the F, G and K classes. However, it is interesting to note that the number of Tycho-2–*MSX* stars detected shows the exact

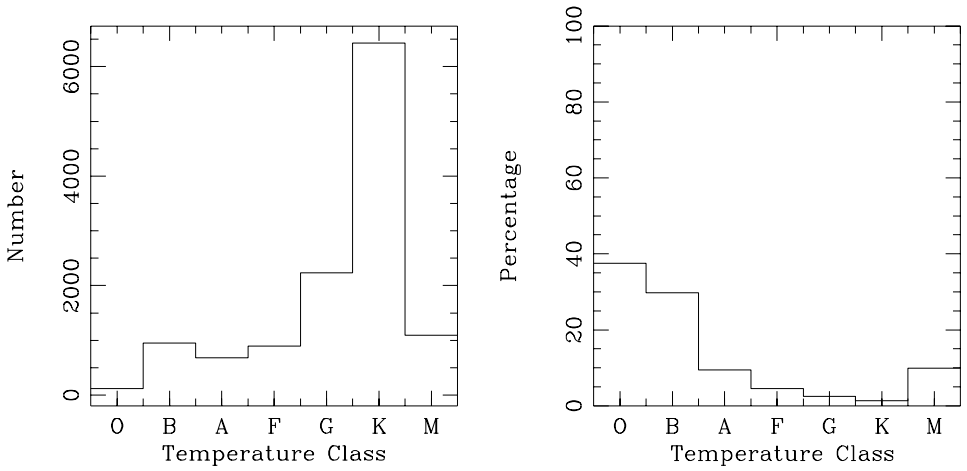

Figure 8. Temperature class distribution of the entire *MSX*–Tycho-2 sample (left) and percentage of stars with excess emission as a function of spectral type (right).

opposite behaviour, indicating that a strong selection effect may be present.

A comparison of the Tycho-2–*MSX* sample with the entire Galactic plane Tycho-2 spectral type catalogue shows that we detect a higher fraction of G and K type compared to other spectral types. The most obvious source of this effect is the sensitivity of the *MSX* satellite. For example, the photospheric emission at 8 μm for all but the brightest O-, B- and A-type stars may be below the detection threshold of *MSX*; we only detect the excess and bright non-excess stars (which are relatively few) thus leading to a higher fraction of excess stars for these spectral types.

5.2 B-type stars with infrared excess

The high fraction (30 per cent) of excess in B-type stars is surprising, as the fraction of Be-type stars in the Bright Star Catalogue is well known to be 15 per cent (Coté & van Kerkwijk 1993). We also noted earlier that there exists a large group of B-type (with and without spectral classification) excess stars with colours that are significantly different to the known Be stars. The nature of these objects is not altogether obvious.

Their H–K colours are quite blue, indicating that these are indeed B-type stars. The normality of the H–K colour indicates that they do not have a great deal of K-band excess. The absence of excess in the K band would seem to lead us away from a free–free emission explanation for these excesses and indicates that these stars are unrelated to the Be stars immediately below them in Fig. 4. The objects are also not particularly reddened, ruling out heavily dust embedded objects and implying the surrounding dust must be relatively optically thin.

We are therefore looking for an optically thin thermally radiating dust mechanism for these stars. Possibilities include: hot post-AGB stars with an optically thin cool detached dust shell, reflection nebulosities, giant stars heating the surrounding interstellar medium dust, weak H II regions and Vega-type stars surrounded by a close warm disc of dust.

To resolve the situation we have looked at the spectral energy distributions of the subsample with *IRAS* detections. We have shown that the objects with intermediate K–[8] colours (2–4) are Herbig stars, Be stars, reflection nebulae and post-AGB stars. The objects with larger K–[8] colours were found to be predominately objects such as post-AGB stars, H II regions and a number of galactic cirrus contaminated fields (some possibly also heated by giant stars). We did not find much evidence for Vega-type disc systems. To complement this we also inspected Galactic Legacy Infrared Mid-Plane Survey Extraordinaire (GLIMPSE; see Benjamin et al. 2003) images for the small number ($\approx$10) of these stars which were within the survey region. The GLIMPSE images mostly showed these objects to be stars within diffuse emission regions and/or associated with star-forming regions. These objects would benefit from ground-based optical follow-up observations to better confirm their nature and to further understand this region of the colour diagram.

5.3 Presentation of the data: data tables

We publish in hard copy (see Table 1) the stars which were not detected by *IRAS* (and therefore should be new identifications), which have full spectral type information and excess K–[8] $>$ 0.75 mag and/or excess emission at other bands. The entire sample (including the other regions discussed in Appendix A) is published in the on-line version of this paper (see Tables S2, S3, S4 and S5).[5] A machine readable format will also be made available at CDS Strasbourg.[6]

5.4 Final remarks

To identify stars with IR excess emission we have positionally correlated the *MSX* PSC with the Tycho-2 star catalogue. We found that a near–mid-IR colour diagram had marked advantages over an optical–mid-IR colour diagram in selecting these objects, specifically in reducing the strong line-of-sight extinction experienced in the direction of the Galactic plane. Using the derived colours of normal stars, selection criteria were developed to identify excess emission sources from the colour diagram. The criteria produced a sample of 1938 stars in the Galactic plane, just over 50 per cent of which were determined to be new identifications of IR excess (i.e. not previously detected by *IRAS*).

The majority of the excess stars were found to be hot stars; a high (30 per cent) fraction of B-type stars with excess was discovered. The IR excesses for a number of these B-type stars were found to be much greater than those of the known Be sample. The known objects in this group were found to be a mixture of Herbig stars, post-AGB stars, reflection nebulae and stars contaminated by galactic cirrus.

The other regions surveyed by *MSX* were also searched for IR excess stars and the same selection criteria were applied (see Appendix A). We publish the entire excess sample on-line (see Table S2) and the brightest new identifications of excess stars in the Galactic plane, in Table 1. These lists should provide a good starting point for future ground-based follow-up observations.

ACKNOWLEDGMENTS

We are grateful to the Royal Astronomical Society, who made the pilot study leading to this work possible by the provision of a Summer Student grant to AJC, and to the UK Particle Physics and Astronomy Research Council (PPARC) for the PhD student grant. We would also like to thank the referee, Michael Egan, for many useful comments. This publication makes use of data products from the 2MASS, which is a joint project of the University of Massachusetts and the Infrared Processing and Analysis Center/California Institute of Technology, funded by the National Aeronautics and Space Administration (NASA) and the National Science Foundation. This research has made use of the NASA/IPAC Infrared Science Archive, which is operated by the Jet Propulsion Laboratory, California Institute of Technology, under contract with NASA. This research has made use of the SIMBAD data base, operated at CDS, Strasbourg, France.

[5] Tables S2, S3, S4, S5 and S6 are only available in the on-line version of this paper (see the 'Supplementary Material' section at the end of this paper). They have the same format as Table 1, aside from an extra column indicating the presence of an *IRAS* counterpart. The entry contains an 'I' if an *IRAS* source was found within 45 arcsec and is empty if none was found. Additionally, Table S6 also includes a column indicating which star-forming region the source is associated with.

[6] See http://vizier.u-strasbg.fr.

Table 1. Tycho-2 stars with IR excess. This table contains the Tycho identifier, Tycho (J2000) position, HD name from the HD catalogue identifications for Tycho-2 stars (Fabricius et al. 2002), spectral type from the Tycho-2 spectral type catalogue (Wright et al. 2003), Tycho B_T and V_T band magnitudes, 2MASS J, H, K near-IR magnitudes, a flag indicating the number of extra 2MASS sources within 6 arcsec of the *MSX* position (# 2MASS), the *MSX* 8-, 12-, 14- and 21-band fluxes (in Jansky), the photometric quality of each of the *MSX* bands (upper limit = 1 to excellent = 4), and finally the excess colour in magnitudes. The excess colour listed is K–[8] unless the entry has superscript J or 21, in which case it is excess J–[8] or K–[21], respectively. The typical errors in the Tycho-2 photometry are 0.05 mag rising to 0.3 mag close to the detection limits. The 2MASS photometry is of higher accuracy than Tycho-2 especially at the fainter end.

TYC1	TYC2	TYC3	Ra (J2000)	Dec. (J2000)	HD	SpType	B_T mag	V_T mag	J mag	H mag	K mag	# 2MASS	F8 Jy	F12 Jy	F14 Jy	F21 Jy	Flux quality	Excess mag
3664	192	1	00 11 37.1	+58 12 42	698	B5II:	7.26	7.11	6.49	6.43	6.33	0	0.39				4 0 0 0	0.79
4034	1319	1	01 24 19.4	+62 49 36		B1:PE(V)	11.51	10.63	8.43	8.13	7.81	1	0.15				3 0 0 0	1.17
4032	17	1	01 58 39.1	+60 37 43		B 1 VE	10.81	10.23	8.32	8.06	7.74	0	0.16				3 0 0 0	1.15
3697	1551	1	02 02 36.4	+59 41 17	12302	B1:V:PE	8.37	8.12	7.22	7.09	6.90	0	0.33				4 0 0 0	1.16
4041	1668	1	02 15 13.0	+64 01 28	13590	B2III	8.33	8.00	7.14	6.99	6.83	0	0.29				3 0 0 0	0.93
3694	1707	1	02 22 06.4	+57 05 25		B 2 III-IVE	10.05	9.83	8.48	8.10	7.55	0	0.29				4 0 0 0	1.53
4049	1502	2	03 16 17.4	+60 02 07	20053	B 3 V	8.43	8.31	7.98	8.02	8.00	1	0.17	2.96			2 1 0 0	1.61
3718	756	1	04 04 21.6	+53 19 44	25348	B1VPNNE	8.44	8.20	7.34	7.16	6.94	0	0.23				4 0 0 0	0.77
2401	381	1	05 09 56.4	+37 00 16	33152	B 1 VE	8.37	8.15	7.69	7.66	7.53	0	0.25				3 0 0 0	1.51
2900	503	1	05 10 48.2	+41 00 10	33232	B 2 VNE	8.29	8.25	7.91	7.81	7.64	1	0.14				2 0 0 0	0.97
2900	112	1	05 13 13.3	+40 11 36	33604	B2V:PE	7.37	7.39	7.44	7.46	7.49	0	0.18				3 0 0 0	1.15
2411	16	1	05 28 07.1	+34 25 26		B 0 IV	9.53	9.40	8.38	8.36	8.32	0	0.16	0.92		3.44	3 1 0 1	1.85
2416	541	1	05 40 59.5	+35 50 46		O 9.5	11.64	10.67	8.38	8.12	7.95	1	1.55	4.57	7.26	19.67	4 4 4 4	3.89
1871	1417	1	05 53 06.1	+26 26 43	39340	B3V	8.18	8.11	7.59	7.58	7.26	0	0.23				4 0 0 0	1.06
1871	1264	1	05 53 59.8	+26 25 21	39478	B 2 V	8.34	8.27	7.81	7.69	7.56	0	0.15				3 0 0 0	1.01
1867	119	1	05 59 53.6	+25 05 19	250028	B2:V:PNNE	9.35	9.14	8.23	8.08	8.16	1	0.19				3 0 0 0	1.88
1321	1207	1	06 00 11.6	+19 11 33	250163	B1,5:V:PNE	10.40	9.83	8.00	7.76	7.44	0	0.18			3.00	2 0 0 1	0.98
1877	931	1	06 08 35.1	+22 37 01	41870	F8IB-G5IB	10.64	9.18	6.74	6.32	6.13	0	0.58				4 0 0 0	0.98
1315	1999	1	06 23 24.7	+15 06 06	44637	B2V	8.27	8.05	7.33	7.25	7.06	0	0.24				4 0 0 0	0.97
750	899	1	06 41 05.9	+09 22 55	261941	A 5 IV	11.33	11.32	10.55	10.15	9.57	0	0.23		0.89		3 0 1 0	3.27
4808	2967	1	06 47 56.9	−05 09 14	49370	B8/9 V	7.57	7.62	7.70	7.75	7.71	0	0.11				2 0 0 0	0.81
5381	2964	1	07 05 35.2	−08 43 43	53667	B0/1 Ib	7.96	7.76	7.13	7.10	6.92	0	0.23				4 0 0 0	0.79
5398	3009	1	07 11 20.8	−10 25 43	55135	B3 Vnne	7.21	7.31	7.38	7.37	7.29	0	0.28				4 0 0 0	1.42
5399	3900	1	07 22 24.8	−10 49 21	57775	B1/2 (I)ne	9.47	9.37	8.34	8.13	7.81	0	0.12				2 0 0 0	0.93
5966	2402	1	07 27 51.0	−16 05 37	59094	B2 (V)NE	8.63	8.50	7.87	7.80	7.54	0	0.16				3 0 0 0	0.98
7119	178	1	07 49 06.0	−31 07 42		F2EIAB	10.40	9.52	7.51	7.10	6.82	0	0.38				4 0 0 0	1.19
7683	1320	1	08 49 31.7	−41 33 49	75607	B3 V	8.85	8.77	8.40	8.35	8.44	1	0.19				3 0 0 0	2.19
7689	1211	1	09 00 22.3	−43 10 26	77320	B2 VNN(E)	5.84	6.03	6.18	6.21	6.05	0	0.34				4 0 0 0	0.69^{J}
8585	3781	1	09 44 07.2	−53 44 43	84523	B3/5 VE	8.01	7.96	7.61	7.53	7.33	0	0.20				4 0 0 0	1.01
8609	2680	1	10 29 47.2	−56 36 46		B 0 VE	10.66	10.12	8.57	8.40	8.02	0	0.14	0.69			2 1 0 0	1.27
8626	2201	1	10 46 12.7	−59 19 05		A6/7 IV/V	8.83	8.55	7.25	7.17	7.14	0	0.20				4 0 0 0	0.90
8957	2047	1	10 47 38.9	−60 37 04	93683	B0/1 (V)NE	8.04	7.98	7.36	7.26	7.05	0	0.25			3.35	4 0 0 1	0.97
8963	1364	1	11 20 27.9	−61 52 36	98678	M5 (III)E	11.58	9.89	5.41	4.47	3.73	0	8.60	5.59	4.17	3.12	4 4 4 3	1.29
8977	3691	1	11 47 35.8	−63 22 38	309036	B 2 II	10.92	10.77	9.97	9.93	9.81	1	0.16				3 0 0 0	3.33
8985	2714	1	11 48 02.2	−66 06 53	102579	K0 V	9.65	8.65	7.08	6.70	6.57	0	0.32			3.01	4 0 0 1	0.80
8974	1391	1	12 03 32.6	−61 05 53	104722	B2 VNE	7.53	7.57	7.10	7.07	6.94	0	0.22				3 0 0 0	0.76
8645	2059	1	12 14 01.8	−59 23 48	106309	B2 III/VNE	7.78	7.86	7.82	7.83	7.62	0	0.18				2 0 0 0	1.17
8994	1920	1	13 10 20.5	−62 41 18	114214	F0 V	10.15	9.39	7.73	7.50	7.35	0	0.19				3 0 0 0	1.00
8994	2766	1	13 14 11.5	−63 22 25	114800	B2 III/VNE	8.05	7.98	7.51	7.36	7.10	0	0.25				4 0 0 0	1.01
8994	3012	1	13 20 35.5	−63 24 43	115746	B2/4 III/V	9.62	9.38	8.08	7.92	7.67	0	0.14				2 0 0 0	0.95
8990	3680	1	13 22 37.9	−60 59 18	116087	B3 V	4.34	4.49	5.24	4.90	4.89	0	0.61				4 0 0 0	0.65^{J}

Table 1 – *continued*

TYC1	TYC2	TYC3	Ra (J2000)	Dec. (J2000)	HD	SpType	B_T mag	V_T mag	J mag	H mag	K mag	# 2MASS	F8 Jy	F12 Jy	F14 Jy	F21 Jy	Flux quality	Excess mag
8995	3220	1	13 27 25.1	−62 38 56	116781	O9/B1 (I)E	7.74	7.67	7.22	6.99	6.72	0	0.44				4 0 0 0	1.23
9003	1626	1	13 28 07.3	−66 16 47	116849	B1 VPE	9.33	9.17	8.72	8.52	8.29	0	0.13				2 0 0 0	1.49
8999	53	1	13 29 54.6	−65 30 07	117111	B2 (V)NE	7.78	7.72	7.28	7.17	7.04	0	0.24		0.51		4 0 1 0	0.98
9016	519	1	13 45 18.4	−66 45 16	119423	B3/5 VNE	7.54	7.59	7.59	7.62	7.59	0	0.12				2 0 0 0	0.81
8676	1771	1	13 50 26.1	−59 44 52	120330	B2/3 VNNE	7.93	7.91	7.51	7.41	7.22	0	0.25				4 0 0 0	1.16
9005	873	1	14 15 09.9	−61 06 42	124340	A0 V	8.42	8.26	7.77	7.75	7.68	0	0.14				2 0 0 0	1.02
9007	747	1	14 35 33.3	−61 00 29	127756	B1/2 VNE	7.69	7.60	7.06	6.93	6.66	0	0.34				4 0 0 0	0.92
8692	1383	1	14 42 05.6	−58 21 34	128937	B3/5 (III)	7.88	7.72	7.34	7.34	7.24	0	0.35				4 0 0 0	1.58
9024	980	1	14 59 21.9	−62 30 32	131925	A3 IV	8.51	8.20	7.45	7.34	7.23	0	0.19				3 0 0 0	0.89
9025	1827	1	15 09 03.3	−61 53 15	133738	B1/2 III/VNE	6.93	6.97	6.66	6.62	6.41	0	0.47				4 0 0 0	1.04
8702	636	1	15 10 59.6	−57 42 43		O 9.5IA	11.51	10.54	7.65	7.35	7.12	0	0.22				4 0 0 0	0.90
8706	14	1	15 15 16.2	−58 10 22	134958	B2 (II)NE	8.48	8.20	6.76	6.57	6.34	0	0.44				4 0 0 0	0.88
8695	2105	1	15 25 55.3	−53 46 15	136968	B5 VNE	8.26	8.25	8.34	8.28	8.14	1	0.12	1.85			2 1 0 0	1.33
8304	641	1	15 42 19.8	−49 59 52	139790	B2 (III)N	8.62	8.57	7.92	7.76	7.55	0	0.16				2 0 0 0	1.02
8321	711	1	15 46 47.4	−52 08 46	140605	B5/7 IV	7.01	7.07	6.96	6.95	6.86	0	0.34				4 0 0 0	1.19
8697	718	1	15 55 29.6	−52 48 15	142170	B8/9 (IV)	9.95	9.92	9.57	9.05	8.54	3	0.13				2 0 0 0	1.62
8322	952	1	16 04 36.2	−51 38 36	143751	B3 II/III	10.23	9.72	8.56	8.45	8.36	0	0.28				4 0 0 0	2.48
8323	688	1	16 12 43.0	−51 35 54	145300	F0 III	10.91	10.44	9.46	9.29	9.21	0	0.21				4 0 0 0	3.00
8319	698	1	16 18 39.4	−49 24 49	146444	B2 VNE	7.67	7.60	7.15	7.09	6.93	0	0.29				4 0 0 0	1.04
8715	1647	1	16 19 14.2	−54 57 42	146463	B3 VNNE	8.05	8.08	7.92	7.90	7.71	0	0.15				3 0 0 0	1.11
8324	1544	1	16 19 42.8	−51 02 04	146630	K2 III	8.57	6.76	3.96	3.21	3.06	0	3.53	2.11	3.76	12.00	4 4 4 4	0.39[21]
8333	1004	1	16 34 43.5	−49 33 09	330950	B1VNE	10.05	9.78	8.66	8.56	8.50	0	0.14		1.01		2 0 1 0	1.85
7862	115	1	16 35 48.7	−42 07 22	149313	B2 IA/BE	9.95	9.48	7.95	7.72	7.48	0	0.17				3 0 0 0	0.97
8333	1429	1	16 36 11.8	−49 15 47	149298	B2 (II)	10.25	9.77	8.12	7.91	7.65	0	0.16				2 0 0 0	1.06
8329	1025	1	16 38 57.7	−47 24 02	149742	K2 III	10.23	8.72	6.22	5.60	5.43	0	0.99	0.94	0.48		4 1 1 0	0.87
8338	2080	1	16 47 51.4	−51 46 04	151083	B2 VN	9.25	9.08	8.21	8.04	7.76	0	0.15				2 0 0 0	1.15
7868	448	1	16 51 00.0	−37 30 52	151771	B8 II/III	6.33	6.23	7.79	7.72	7.66	1	0.32				4 0 0 0	1.92
8335	1898	1	17 00 28.7	−49 15 14	153222	B1 IB/IIIE	9.17	8.90	8.38	8.30	8.18	0	0.15				2 0 0 0	1.61
7372	375	1	17 05 52.8	−36 35 17	154243	B3 VNNE	8.28	8.08	7.29	7.14	6.92	0	0.29			2.42	4 0 0 1	1.02
7878	1149	1	17 16 17.6	−42 20 20	155896	B2/3 (V)NNE	7.03	6.96	6.20	6.12	5.99	0	0.63				4 0 0 0	0.97
7374	641	1	17 18 38.3	−36 05 13	156369	A2 V	8.94	8.32	6.76	6.61	6.44	0	0.37				4 0 0 0	0.83
7874	809	1	17 19 16.8	−39 48 25	156409	B2 (II)NE	9.18	8.78	7.94	7.80	7.59	0	0.18				3 0 0 0	1.20
7384	16	1	17 37 30.9	−35 19 59	159684	B2 VNE	8.63	8.24	6.80	6.60	6.34	0	0.53				4 0 0 0	1.07
6840	1414	1	17 48 35.5	−29 57 28	316341	B0,5V(PE)?	9.74	9.15	7.60	7.34	6.96	1	0.26				4 0 0 0	0.85
7377	827	1	17 49 08.6	−31 17 16	161839	B5/7 II/III	9.77	9.64	7.63	6.58	6.35	1	1.33	0.89	1.04		4 1 2 0	2.09
6841	1403	1	17 59 47.6	−23 48 58	163955	B9 V	4.70	4.72	4.84	4.61	4.47	0	1.29	0.72	0.68		4 1 2 0	0.78[J]
7382	1514	1	17 59 56.4	−33 24 29	163868	B2/3 (V)NE	7.30	7.35	7.14	7.06	6.88	0	0.31				3 0 0 0	1.07
6846	437	1	18 04 39.6	−26 01 07	164950	B3/5 II	9.43	9.13	8.07	8.00	7.77	0	0.13				2 0 0 0	1.01
6263	2940	1	18 04 43.2	−20 56 44	165014	F2 V	10.11	9.33	7.42	7.04	6.77	0	1.08	0.78	0.76		4 1 1 0	2.27
6259	2481	1	18 05 58.8	−19 57 13	165285	B1/2 (I)NN(E)	8.89	8.45	7.02	6.78	6.48	0	0.44				4 0 0 0	1.00
6263	2328	1	18 07 11.4	−21 26 38	165516	B1/2 IB	6.32	6.26	6.00	5.99	5.90	0	0.60	0.88			4 1 0 0	0.83
6272	2074	1	18 08 27.1	−19 52 07	165783	B3/5 IB	8.69	8.37	7.45	7.28	7.09	0	0.22				4 0 0 0	0.92

Table 1 – *continued*

TYC1	TYC2	TYC3	Ra (J2000)	Dec. (J2000)	HD	SpType	B_T mag	V_T mag	J mag	H mag	K mag	# 2MASS	F8 Jy	F12 Jy	F14 Jy	F21 Jy	Flux quality	Excess mag
6268	2490	1	18 10 18.3	−18 11 41	166188	B3 (II)E	9.31	8.98	7.68	7.52	7.28	0	0.23				4 0 0 0	1.09
6268	212	1	18 10 38.8	−17 44 02	166288	B5 IB	10.38	10.06	9.06	8.99	8.92	0	0.28				4 0 0 0	3.03
6268	620	1	18 10 42.1	−17 55 05	166289	K1/2 (III)	11.17	9.31	6.35	5.64	5.45	0	1.45	1.11	1.13	1.89	4 2 1 1	1.30
6268	637	1	18 12 33.9	−18 23 51	166691	B8 II	8.23	8.20	7.92	7.89	7.43	0	1.23	1.61	1.39		4 3 3 0	3.00
5689	949	1	18 19 04.9	−13 48 20		B 1.5V	11.12	10.69	9.58	9.45	9.31	1	0.44	1.05	1.75	2.44	4 1 3 2	3.88
5689	815	1	18 19 05.6	−13 54 50		B1V	9.73	9.50	8.71	8.65	8.61	0	0.21	0.90	1.17	4.21	4 1 3 4	2.43
6269	1768	1	18 19 27.2	−18 13 10	168229	B2/3 IB/IIE	8.86	8.68	7.90	7.76	7.50	0	0.17				2 0 0 0	0.98
6265	875	1	18 20 22.2	−15 48 29	168446	G8 V	10.76	9.91	8.21	7.86	7.77	0	0.26				4 0 0 0	1.79
6269	980	1	18 22 50.3	−17 26 48	313240	B2 IV(NN)	9.51	9.34	8.57	8.44	8.25	1	0.12				2 0 0 0	1.36
6274	832	1	18 27 12.0	−18 57 13	169805	B2 VNE	8.18	8.04	7.42	7.30	7.05	0	0.30				4 0 0 0	1.16
5124	2597	1	18 36 07.8	−06 44 31	171610	K2 III	8.67	7.09	4.77	3.66	4.42	0	1.75	0.83	0.55	9.55	4 4 4 1	0.86
5700	654	1	18 39 39.8	−11 52 42	172252	B0 V:e	10.12	9.63	7.93	7.74	7.49	0	0.17				3 0 0 0	0.98
5125	325	1	18 44 33.3	−07 06 38	173219	B0 Iae	8.04	7.90	7.14	7.05	6.80	0	0.32				4 0 0 0	0.99
1044	195	1	19 04 08.0	+11 06 24	230579	B1,5:IV:NE	9.72	9.19	7.74	7.54	7.26	1	0.22				4 0 0 0	1.02
2139	1057	1	19 42 50.9	+22 33 45	344800	B2V:NNE	10.42	10.05	8.90	8.78	8.49	0	0.10	1.13			2 1 0 0	1.39
2682	3762	1	19 59 55.2	+37 02 34	189687	B3V	4.97	5.12	5.41	5.48	5.49	0	0.85				4 0 0 0	0.83
2679	717	1	20 09 58.4	+35 29 45	228041	B0,5V:E	9.35	9.05	7.87	7.64	7.36	0	0.19				3 0 0 0	0.98
2683	1156	1	20 13 33.0	+36 19 42	192445	B0,5III	7.03	7.08	7.13	7.08	6.91	0	0.32				4 0 0 0	1.13
2683	174	1	20 13 50.3	+36 37 22	228438	B0(IV)	8.77	8.41	7.18	7.05	6.76	0	0.30				4 0 0 0	0.85
2686	693	1	20 33 05.1	+31 39 25	195907	B 1.5V	7.82	7.79	7.46	7.43	7.28	0	0.19				2 0 0 0	0.96
3171	1117	1	20 54 22.3	+40 42 10	199218	B 8 V:NN	6.59	6.69	6.69	6.73	6.70	1	0.26				4 0 0 0	0.77
3575	553	1	20 57 59.4	+46 28 00		M2IA	11.66	8.48	2.77	1.74	1.29	0	113.22	119.72	80.39	86.49	4 4 4 4	1.76
3970	673	1	21 24 30.3	+55 22 00	204116	B1VE	8.13	7.60	6.21	5.96	5.63	0	0.88		0.89		4 0 1 0	0.88
3194	2107	1	21 25 02.4	+44 27 06		B1,5V:PNNE	9.47	8.94	7.43	7.21	6.94	0	0.26				4 0 0 0	0.91
3979	1275	1	21 36 59.6	+58 08 24	239712	B 2 VNNE	9.00	8.59	7.54	7.48	7.28	0	0.23				2 0 0 0	1.12
3986	1670	1	22 18 45.6	+56 07 33	211853	B0:I:+WR	9.44	9.06	7.78	7.60	7.41	0	0.18	1.18	1.09		3 1 1 0	1.00
4282	933	1	22 56 42.6	+62 37 29	217061	B1V	9.51	8.88	7.26	7.13	7.03	0	0.64	1.85	2.71	5.70	4 2 4 4	2.03
4011	773	1	23 20 34.3	+58 16 39	220116	B0,5VPE	9.26	8.68	7.59	7.50	7.36	0	0.17				2 0 0 0	0.90
4285	1070	1	23 49 53.1	+62 12 50	223501	B 1 VNE	7.73	7.74	7.74	7.77	7.67	0	0.18				3 0 0 0	1.28

REFERENCES

Alksnis A., Balklavs A., Dzervitis U., Eglitis I., Paupers O., Pundure I., 2001, Baltic Astron., 10, 1

Aumann H. H., Beichmann C. A., Gillet F. C., de Jong T., Houck J. R., Low F. J., Neugebauer G., Walker R. G., Wesselius P. R., 1984, ApJ, 278, L23

Beichman C., Neugebauer G., Habing H. J., Clegg P. E., Chester T. J., eds, 1988, *IRAS* Catalogues and Atlases Explanatory Supplement, NASA RP-1190, Vol. 1. GPO, Washington, DC

Benjamin R. A. et al., 2003, PASP, 115, 953

Chengalur J. N., Lewis B. M., Eder J., Terzian Y., 1993, ApJS, 89, 189

Cohen M., Schwartz D. E., Chokshi A., Walker R. G., 1987, AJ, 93, 1199

Cohen M., Hammersley P. L., Egan M. P., 2000, AJ, 120, 3362

Coté J., van Kerkwijk M. H., 1993, A&A, 274, 870

Cutri R. M. et al., 2003, 2MASS All-Sky Catalogue of Point Sources

Draine B. T., Lee H. M., 1984, ApJ, 285, 89

Egan M. P., van Dyk S. D., Price S. D., 2001, AJ, 122, 1844

Egan M. P., Price S. D., Kraemer K. E., 2003, The *Mid-Course Space Experiment* Point Source Catalogue Version 2.3 Explanatory Guide (AFRL-VS-TR-2003-1589)

ESA, 1997, The Hipparcos, Tycho Catalogues, ESA SP-1200, Vol., 1–17 (ESA97)

Fabricius C., Makarov V., Knude J., Wycoff G. L., 2002, A&A, 386, 709

Hoffleit D., Warren W. H., Jr, 1991, Bright Star Catalogue, 5th revised edn. Yale University Observatory, New Haven

Hog E. et al., 2000, A&A, 355, 27

Jura M., 1999, ApJ, 515, 706

Koornneef J., 1983, A&A, 128, 84

Kraemer K. E., Shipman R. F., Price S. D., Mizuno D. R., Kuchar T., Carey S. J., 2003, AJ, 126, 1423

Lumsden S. L., Hoare M. G., Oudmaijer R. D., Richards D., 2002, MNRAS, 336, 621

Oudmaijer R. D., van der Veen W. E. C. J., Waters L. B. F. M., Trams N. R., Waelkens C., Engelsmann E., 1992, A&AS, 96, 625

Plets H., Waelkens C., Oudmaijer R. D., Waters L. B. F. M., 1997, A&A, 323, 513

Pottasch S. R., Olling R., Bignell C., Zijlstra A. A., 1988, A&A, 205, 248

Price S. D., Egan M. P., Carey S. J., Mizuno D. R., Kuchar T. A., 2001, AJ, 121, 2819

SAO Staff, 1966, Star Catalogue: Positons and Proper Motions of 258 997 Stars for Epoch and Equinox of 1950.0, Publ. Smithsonian Inst. of Washington DC, 4562

Schmidt-Kaler Th., 1982, Stars and Star Clusters, in Landolt-Bornstein, New Series, Vol. VI, 2b. Springer-Verlag, Berlin, p. 1

Stencel R. E., Backman D. E., 1991, ApJS, 75, 905

Thé P. S., de Winter D., Perez M. R., 1994, A&AS, 104, 315

Walker H. J., Cohen M., 1988, AJ, 95, 1801

Waters L. B. F. M., Waelkens C., 1998, ARA&A, 36, 233

Waters L. B. F. M., Coté J., Aumann H. H., 1987a, A&A, 172, 225 (WCA)

Waters L. B. F. M., Coté J., Lamers H. J. G. L. M., 1987b, A&A, 185, 206

Wright C. O., Egan M. P., Kraemer K. E., Price S. D., 2003, AJ, 125, 359

van der Veen W. E. C. J., Habing H. J., 1988, A&A, 194, 125

van Winckel H., 2003, ARA&A, 41, 391

Zhang P., Chen P. S., Yang H. T., 2005, NewA, 10, 325

Zuckerman B., 2001, ARA&A, 39, 549

APPENDIX A: OTHER *MSX* CATALOGUES

The *MSX* satellite observed a number of regions in addition to the Galactic plane and the *IRAS* gaps. These were generally regions of high source density that were labelled as confused by *IRAS* and included the Magellanic Clouds, several star-forming regions and a number of extended objects such as galaxies. We have undertaken a search for excess stars in the *IRAS* gaps and all of the above regions except the galaxies. The results of these searches are discussed below.

A positional correlation of the non-plane ($|b| > 6^\circ$) *MSX* catalogue sources with the Tycho-2 star catalogue found 5898 (68 per cent) *MSX* sources within 6 arcsec of a Tycho-2 star. The non-plane *MSX* catalogue contains both the *IRAS* gap (Appendix A1) and the Large Magellanic Cloud (LMC) surveys. We discuss the LMC stars separately in Appendix A2 and define these to be within a 14° square (272°, −26° to 286°, −40°) around the LMC's galactic coordinate position. Of the non-plane sample, 753 (12 per cent) were within 45 arcsec of an *IRAS* source. A small fraction (20 per cent) of these *IRAS* associations are LMC stars.

A1 *IRAS* gaps

5364 *MSX*–Tycho-2 *IRAS* gap stars are identified. 66 per cent (3522) of these have spectral type information and 5215 have 2MASS counterparts. A near–mid-IR colour diagram is shown in Fig. A1. Although much less reddened, the *H–K K*–[8] colours are similar to the Galactic plane sample. The same excess determination process was applied to the *IRAS* gaps, and we identify 95 (87 warm and eight hot) IR excess stars in this region. 22 of these excess stars were found to be within 45 arcsec of an *IRAS* source; these were found to be at the edges of the *IRAS* gap regions.

The star with large excess is the variable star ST Pup; the other stars with excesses fall neatly into the groups we have previously discussed for the Galactic plane. These stars are published in Table S3.

A2 Magellanic Clouds

The LMC was found to contain 534 *MSX*–Tycho-2 sources; of these, 523 have 2MASS counterparts and 333 have spectral type information. An *H–K K*–[8] colour diagram of the sample is shown in Fig. A1. These stars are mainly G, K and M giant type stars. However, a comparison of *MSX* and 2MASS observations of the LMC by Egan, van Dyk & Price (2001) indicated that the spatial distributions of these stars are more likely galactic foreground objects rather than LMC stars. We identify 24 warm excess stars, 10 of which were within 45 arcsec of an *IRAS* source. The LMC IR excess stars can be found in Table S4.

The excess stars are nearly all supergiants; the objects with $H–K > 0.70$ are well-known Be supergiants, and their extreme *H–K* colours are a result of strong *K*-band excess from the star's hot dust disc. Interestingly, the colours of the Be supergiants overlap with the Herbig stars observed in the Galactic plane (see Fig. 4). The stars with blue $H–K < 0.2$ colours and large excesses are young massive stars. The lower excess stars are late-type stars with circumstellar material and the well-known luminous blue variable, S Dor.

A correlation of the Small Magellanic Cloud (SMC) *MSX* mini-catalogue (containing 243 sources) with Tycho-2, yielded 55 associations. 54 of these stars have 2MASS counterparts and 42 have spectral types. An *H–K K*–[8] colour diagram of the SMC sample is shown in Fig. A1. We identify four excess stars (four warm). Of these, none was detected by *IRAS*. The excess stars found in the SMC were known or suspected late-type supergiants. The SMC IR excess stars are listed in Table S5.

A3 Star-forming regions outside the Galactic plane

Here we discuss only the regions that are outside the Galactic plane, and hence are not part of the Galactic plane survey discussed earlier.

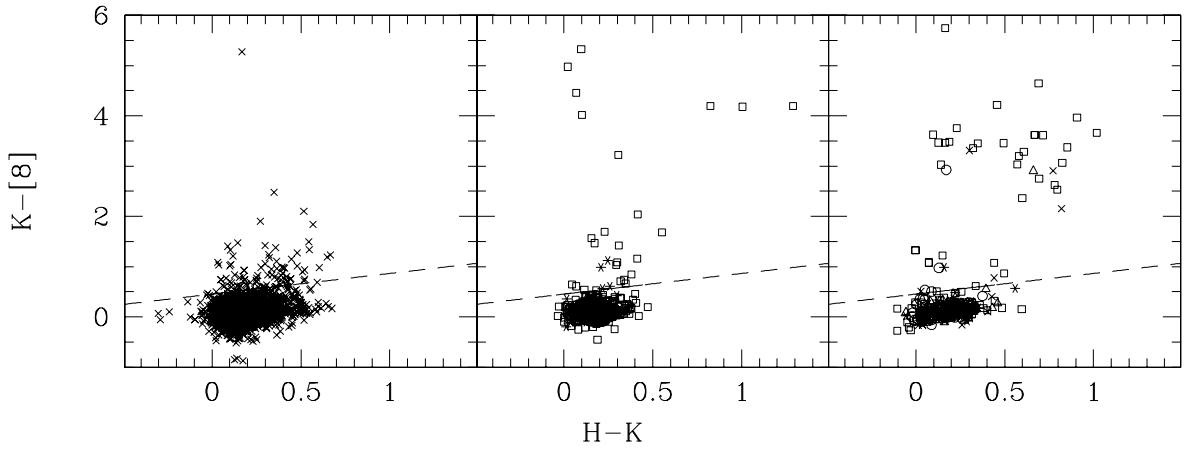

Figure A1. Near–mid-IR colour diagram of the *IRAS* gaps (5215 stars; left), the LMC (squares; 523 sources) SMC (asterisks; 54 sources; centre) and the non-Galactic plane star-forming regions observed by *MSX* (right). In the right-hand panel, the different regions are indicated by the following symbols: times symbols, G159.6–18.5; triangles, G300.2–16.8; squares, Orion nebula (A and B); circles, Pleiades; asterisks, S263. The excess cut-off is shown in all the diagrams by a dashed line.

The following star-forming regions were imaged during the *MSX* mission (see Kraemer et al. 2003, for full details).

The Orion nebula (A and B), the H II region S263, the *IRAS* loop G159.6–18.5 associated with the Perseus molecular cloud, the Pleiades star cluster and G300.2–16.8, an isolated cloud in Chamaeleon associated with IRAS 11538–7855. We have searched the *MSX* Point Source mini-catalogues associated with each of the regions for Tycho-2 and 2MASS counterparts. The searches found 160 *MSX*–Tycho-2–2MASS sources in Orion, 41 in S263, 53 in G159.6–18.5, 51 in the Pleiades and 54 in G300.2–16.8.

We show the K–[8] H–K colour diagram for these star-forming regions in Fig. A1. The majority (78 per cent) of the IR excess stars in the star-forming regions are found in the Orion nebula. In the star-forming regions we identify 51 excess stars (46 warm, four hot, one cool). Of theses sources, approximately 80 per cent were within 45 arcsec of an *IRAS* point source. The excess stars tend to split into the Herbig stars with $H-K > 0.5$ and variable stars of Orion type $H-K < 0.5$. The IR excess stars found in the star-forming regions are in Table S6.

SUPPLEMENTARY MATERIAL

The following supplementary material is available for this article on-line.

Table S2. The entire Galactic plane sample of Tycho-2 stars with IR excess.

Table S3. *IRAS* gap Tycho-2 stars with IR excess.

Table S4. LMC Tycho-2 stars with IR excess.

Table S5. SMC Tycho-2 stars with IR excess.

Table S6. Tycho-2 stars with IR excess in star-forming regions (SFRs).

This paper has been typeset from a TEX/LATEX file prepared by the author.